Ultrasound in Med. & Biol., Vol. 42, No. 10, pp. 2423–2435, 2016

0301-5629/$ - see front matter

http://dx.doi.org/10.1016/j.ultrasmedbio.2016.05.021

● *Original Contribution*

SHEAR WAVE ELASTOGRAPHY QUANTIFIES STIFFNESS IN *EX VIVO* PORCINE ARTERY WITH STIFFENED ARTERIAL REGION

Erik Widman,*† Elira Maksuti,*† Carolina Amador,‡ Matthew W. Urban,‡§ Kenneth Caidahl,† and Matilda Larsson*†

*Department of Medical Engineering, School of Technology and Health, KTH Royal Institute of Technology, Stockholm, Sweden; †Department of Molecular Medicine and Surgery, Karolinska Institutet, Solna, Sweden; ‡Department of Physiology and Biomedical Engineering, Mayo Clinic College of Medicine, Rochester, Minnesota, USA; and §Department of Radiology, Mayo Clinic College of Medicine, Rochester, Minnesota, USA

(*Received* 17 *February* 2016; *revised* 17 *May* 2016; *in final form* 31 *May* 2016)

Abstract—Five small porcine aortas were used as a human carotid artery model, and their stiffness was estimated using shear wave elastography (SWE) in the arterial wall and a stiffened artery region mimicking a stiff plaque. To optimize the SWE settings, shear wave bandwidth was measured with respect to acoustic radiation force push length and number of compounded angles used for motion detection with plane wave imaging. The mean arterial wall and simulated plaque shear moduli varied from 41 ± 5 to 97 ± 10 kPa and from 86 ± 13 to 174 ± 35 kPa, respectively, over the pressure range 20–120 mmHg. The results revealed that a minimum bandwidth of approximately 1500 Hz is necessary for consistent shear modulus estimates, and a high pulse repetition frequency using no image compounding is more important than a lower pulse repetition frequency with better image quality when estimating arterial wall and plaque stiffness using SWE. (E-mail: erik.widman@sth.kth.se)

Key Words: **Artery, Arteriosclerosis, Atherosclerosis, Elasticity, *Ex vivo*, Plaque, Phase velocity, Shear wave elastography, Ultrasound.**

INTRODUCTION

According to the World Health Organization (2011), ischemic stroke was the second leading cause of mortality in 2012, with an estimated 6.7 million deaths worldwide. Approximately 15%–30% of ischemic strokes are caused by carotid atherosclerotic disease (Kan et al. 2012), which has been associated with the development of cerebrovascular events because of the rupture of vulnerable carotid plaques (Salem et al. 2013). Moreover, an increase in arterial stiffness can be an early predictor of mortality caused by cardiovascular diseases (Quinn et al. 2012; Vlachopoulos et al. 2010). Arterial stiffness can be measured with regional pulse wave imaging (Luo et al. 2012) or global pulse wave velocity (Caro and Harrison 1962), which provides a stiffness measure for the arterial system. However, pulse wave velocity suffers from several limitations and does not take into consideration dynamic vessel dimensions or stress-dependent stiffness variations (Hamilton et al. 2007). Additionally, there has also been an attempt to use non-invasive vascular elastography to characterize arterial stiffness by measuring the strain of the arterial wall (Maurice et al. 2008).

Atherosclerosis can lead to the formation of arterial plaques. Characteristics of vulnerable plaques are surface ulcerations, intra-plaque hemorrhage, a necrotic core, a thin fibrous cap and neovascularization (Carr et al. 1996; Dunmore et al. 2007). Current clinical first-level screening for vulnerable plaques is based on visual assessment of carotid ultrasound duplex scanning (Saba et al. 2012), where the degree of stenosis and plaque morphology are used to determine the appropriate therapy (Barnett et al. 1998). However, visual assessment is vulnerable to both human error and inter-subjectivity, and several studies have reported that the degree of lumen stenosis is an indirect indicator of plaque vulnerability (Naghavi et al. 2003a, 2003b; Schwarz et al. 2013).

Address correspondence to: Erik Widman, School of Technology and Health, KTH Royal Institute of Technology, Alfred Nobels Allé 10, Huddinge 141 52, Sweden. E-mail: erik.widman@sth.kth.se

It has been suggested that assessment of the mechanical properties of plaques to determine plaque vulnerability would be a better measure than visual assessment of the degree of lumen stenosis. Thus, accurate quantitative techniques for characterization of mechanical properties of plaques are needed.

Many attempts have been made to use ultrasound-based methods to characterize plaque composition, such as gray-scale median (Kanber et al. 2013), contrast-enhanced ultrasound imaging (Muller et al. 2014), strain imaging by speckle tracking (Widman et al. 2015a), thermal strain imaging (Mahmoud et al. 2013), intravascular ultrasound elastography (Zhang et al. 2011) and acoustic radiation force impulse (ARFI) imaging (Allen et al. 2011; Czernuszewicz et al. 2015), but these techniques have various technical limitations (high variability) or suffer from conflicting studies of effectiveness and are not part of clinical practice. Shear wave elastography (SWE) has been reported to be reproducible for *in vivo* plaque stiffness measurements (Ramnarine et al. 2014) and to accurately measure the stiffness of simulated plaques in a phantom setup compared with mechanical testing (Widman et al. 2015b). Therefore, SWE has the potential to assess plaque vulnerability in a clinical setting in the future.

Elasticity imaging in the determination of tissue stiffness has become more common in recent years. SWE uses the shear modulus of the tissue as the imaging contrast mechanism. In SWE, an acoustic radiation force (ARF) push non-invasively generates shear waves in the tissue, while ultrasonic methods are used to measure the shear wave propagation speed. The technique has been applied in breast (Tanter et al. 2008), liver (Muller et al. 2009), thyroid (Mehrmohammadi et al. 2015), muscle (Gennisson et al. 2010), kidney (Gennisson et al. 2012), arterial wall (Couade et al. 2010) and myocardium (Song et al. 2013; Vejdani-Jahromi et al. 2015), where it has successfully detected physiologic changes in tissue stiffness that may not have been detected by traditional B-mode imaging.

In one case study on the use of SWE in the arterial wall *in vivo* (Couade et al. 2010), the ARF push length and number of compounded angles were not optimized, the technique's sensitivity was not evaluated, arterial plaque stiffness was not estimated, nor were the results validated. The aim of our study was to investigate the effect of optimizing the ARF push length and number of compounded angles to obtain better shear modulus estimates using phase velocity analysis. Increasing the number of data points (by generating a shear wave with a large bandwidth) when fitting a wave propagation model to the shear wave phase velocity data provides a better fit and more reliable shear modulus estimates. Therefore, it is important to optimize ARF push length and number of compounded angles such that the bandwidth of the shear wave is maximized to provide an accurate shear modulus estimate. Ramnarine et al. (2014) performed an *in vitro* reproducibility study assessing plaque stiffness, but the study did not consider that shear waves with different frequencies propagate at different speeds within the plaque, resulting in inaccurate stiffness estimates. Moreover, a commercial ultrasound machine that does not have a shear wave algorithm optimized for plaque characterization or measurement of arterial wall stiffness was used (Ramnarine et al. 2014). It has been reported that phase velocity analysis is necessary to estimate plaque stiffness when using SWE to obtain reliable estimates (Maksuti et al. 2016; Widman et al. 2015b).

Waves propagating in the arterial wall can be considered guided waves with relatively high propagation velocities, 3–7 m/s (Bernal et al. 2011; Couade et al. 2010). To measure these fast waves appropriately, plane wave imaging can be used to achieve high frame rates over the full field of view. Coherent compounding of multiple plane waves can be used to increase the signal-to-noise ratio (SNR) of the resulting ultrasound signals (Montaldo et al. 2009).

The long-term clinical goal of using SWE to characterize plaques is to develop a threshold criterion to evaluate the likelihood of plaque rupture, allowing physicians to determine the most suitable treatment for the patient. The work presented in this article takes steps toward reaching this goal. The objective of this study was to find the optimal ARF push length and angle compounding settings that maximize the bandwidth for conducting phase velocity analysis on shear waves propagating in the arterial wall with regions of increased arterial stiffness or simulated stiff plaques and to use these settings to quantify arterial and a simulated plaque stiffness in an *ex vivo* setting with realistic *in vivo* intraluminal pressures. Furthermore, a mathematical model was created based on our results to estimate the arterial wall and simulated plaque stiffness based on pressure.

BACKGROUND

Ultrasound-based elastography methods can be categorized by excitation duration as quasi-static, transient and harmonic elastography (Doherty et al. 2013b). When characterizing plaque, it is advantageous to select a method that excites the plaque in an offset position (the ARF push is located beside the plaque), such as SWE or Supersonic Shear imaging, to minimize the risk of plaque rupture. Furthermore, these elastography techniques have reported to be repeatable in a phantom setup (Dillman et al. 2015).

In transient SWE, the shear waves are non-invasively generated through an ARF push that creates

a propagating shear wave traveling orthogonally with respect to the excitation ultrasound beam. The speed of the propagating shear wave is proportional to the shear modulus of the tissue, which is considered to be synonymous with stiffness in this article. When investigating large media such as breast or liver, the tissue is considered an incompressible, homogeneous, isotropic, infinitely large medium where the shear modulus (μ) can be approximated as

$$\mu = \rho c_g^2 \tag{1}$$

where ρ is the mass density, and c_g is the shear wave group velocity. However, these assumptions are not valid when characterizing plaque or the arterial wall.

Plaques can be of homogeneous or heterogeneous composition (Carr et al. 1996; Davis 2005; Saba et al. 2014), and the arterial wall consists of the tunica adventitia, tunica media and tunica intima layers (Schmidt and Thews 1989). Moreover, plaques and arteries are not infinitely large media, and arteries have been found to be anisotropic (Weizsacker and Pinto 1988). Conflicting studies have considered plaques and arteries to be compressible (Loree et al. 1992) and incompressible (Tang et al. 2004) when creating artery models with plaques. Because all of the assumptions are not met, phase velocity analysis must be taken into consideration, as group velocity analysis has been reported to underestimate the shear modulus (Widman et al. 2015b).

In our experiment, a stiffened arterial region was created and considered a model for increased arterial stiffness, as was a model of a stiff plaque embedded in the arterial wall. For the shear wave propagation analysis in our experimental setup, the artery was modeled as a thin hollow cylinder. Many groups have modeled the complex shear wave propagation in the artery as a fundamental anti-symmetric Lamb wave mode traveling through an infinite plate, as the shear wave propagation in a hollow cylinder is difficult to solve analytically (Bernal et al. 2011; Couade et al. 2010; Widman et al. 2015b). Bernal et al. (2011) provides a comprehensive derivation of a Lamb wave dispersion equation for a homogeneous elastic plate submerged in incompressible water-like fluid:

$$\begin{aligned} &4k_L^3\beta\cosh(k_L h)\sinh(\beta h) - \left(k_s^2 - 2k_L^2\right)^2 \\ &\sinh(k_L h)\cosh(\beta h) = k_s^4\cosh(k_L h)\cosh(\beta h) \end{aligned} \tag{2}$$

$$k_L = \frac{\omega}{c_L},\quad k_s = \omega\sqrt{\frac{\rho}{\mu}},\quad \beta = \sqrt{k_L^2 - k_s^2} \tag{3}$$

Here, ρ is the mass density, ω is the angular frequency, c_L is the frequency-dependent Lamb wave velocity, k_L is the Lamb wavenumber, k_s is the shear wave number, h is the half-plate thickness and μ is the shear modulus. The model is similar to a shear wave propagating in a thin hollow cylinder model at higher frequencies (>1 kHz) and has been reported to provide accurate estimates of arterial and plaque stiffness when the curve fit is to the upper half-bandwidth of the fundamental mode of the shear wave (Widman et al. 2015b).

It is desirable to maximize the bandwidth of the propagating shear wave to overcome the discrepancies at lower frequencies (<1 kHz) between the models of a Lamb wave propagating through a thin plate submerged in water and a shear wave propagating in a hollow cylinder. The increased bandwidth may result in a more accurate shear modulus estimate when curve fitting the equation for an anti-symmetric Lamb wave propagating in a thin plate to the upper half-bandwidth of the shear wave phase velocity curve. The bandwidth is dependent on the length of the ARF push, and the relationship between push length and bandwidth for a shear wave propagating in an artery or plaque has to be investigated to study how the shear modulus estimate is affected as the bandwidth decreases.

Furthermore, increasing the number of plane wave imaging angles improves the image quality at the expense of a reduced pulse repetition frequency (PRF). The PRF is obtained by computing

$$\mathrm{PRF} = \frac{1}{I_a t_i} \tag{4}$$

where I_a is the number of imaging angles, and t_i is the time required for each imaged acquisition. It is uncertain if maximizing the PRF when tracking the wave propagation in a vessel wall is more important than increasing the image quality by compounding multiple imaging angles at the expense of a reduced PRF.

Finally, it is desirable to quantify the sensitivity of SWE to determine how sensitive the technique is to small changes in arterial and plaque stiffness. This could determine if the technique is appropriate for detecting early-onset atherosclerosis and assisting in plaque characterization.

METHODS

A porcine aorta with a stiffened region was used as a model of the human carotid artery with early plaque formation. The artery was connected to a fixture and pressurized with a water column. Thereafter, the shear wave bandwidth was measured with respect to the push length and number of compounded angles. After the optimal settings for obtaining the maximum bandwidth were achieved, five porcine aortas with stiffened regions were used as models for human carotid arteries with regions of increased arterial stiffness or stiff plaques and

were tested at various static pressures at which the shear modulus was measured in both the arterial wall and simulated plaque. Thereafter, one of the arteries was incrementally stiffened to evaluate the sensitivity of the technique to small changes in arterial stiffness. The experimental setup is outlined in Table 1.

Experimental setup

Five thoracic aortas were surgically removed from small Swedish Yorkshire pigs (mean weight: 35 ± 1.6 kg, two male, three female) after the pigs had been sacrificed for medical education. The arteries were placed in 0.9% saline and frozen at approximately −23°C. The specimens were thawed in a refrigerator (approximately 9°C) for 48 h before the experiments. Fascia surrounding the arteries was removed, and the arteries were cut to a length of approximately 10 cm (Fig. 1a). Half of each artery was soaked in a bath of 36.5% formaldehyde solution (Sigma-Aldrich, St. Louis, MO, USA) for 20 min to simulate a region with increased arterial stiffness or a stiff plaque. The midpoints of the specimens were highlighted with a marker before soaking to visually distinguish the border between the unstiffened and stiffened regions. Next, the intercostal arterioles were glued shut with universal hybrid glue (Loctite, Düsseldorf, Germany), and the specimens were attached to a fixture using thread with the intercostal arterioles facing downward, pressurized with saline and checked for leaks. The arteries were stretched approximately 5% of their unpressurized length to minimize buckling during pressurization. The fixture was connected to a pressure sensor followed by a saline-filled water column and placed in a saline bath, as illustrated in Figure 1b.

Data acquisition

The artery's lumen diameter and wall thickness were measured with an Aixplorer ultrasound machine (Supersonic Imagine, Aix-en-Provence, France) using a SL15-4 linear array transducer fixed 1 cm above the artery. Long-axis images were acquired with a center frequency of 7.25 MHz, a 3.5-cm depth and a focal point on the anterior arterial wall, using harmonic imaging with no image compounding, resulting in a frame rate of 32 Hz. The lumen diameter was measured at 60 mmHg at three locations in both ends of the artery and averaged. The anterior wall thickness was measured from 20 to 120 mmHg in increments of 20 mmHg at three locations within the shear wave propagation region and averaged together, as the arterial wall thickness was an important parameter in the post- processing algorithm.

The SWE experiments were performed with a Verasonics acquisition system (Verasonics, Kirkland, WA, USA) using a linear L7-4 probe (Philips Healthcare, Andover, MA) with an in-house script to generate shear waves with an ARF push and collect in-phase and quadrature (IQ) data using plane wave imaging. The transducer was fixed 1 cm above the artery, and the anterior arterial wall was excited with a single focused ARF push (center

Table 1. Summary of experimental setups

Experiment	Number of arteries	Upper-limit frequency (Hz)	Pressure (mmHg)	Measured variable
Push length	1	None	60, 120	Bandwidth, μ
Compounded angles	1	None	60, 120	Bandwidth
Pressure	5	1700	20–120	μ, RMSE
Sensitivity	1	1700	60	μ

μ = shear modulus; RMSE = root mean square error.

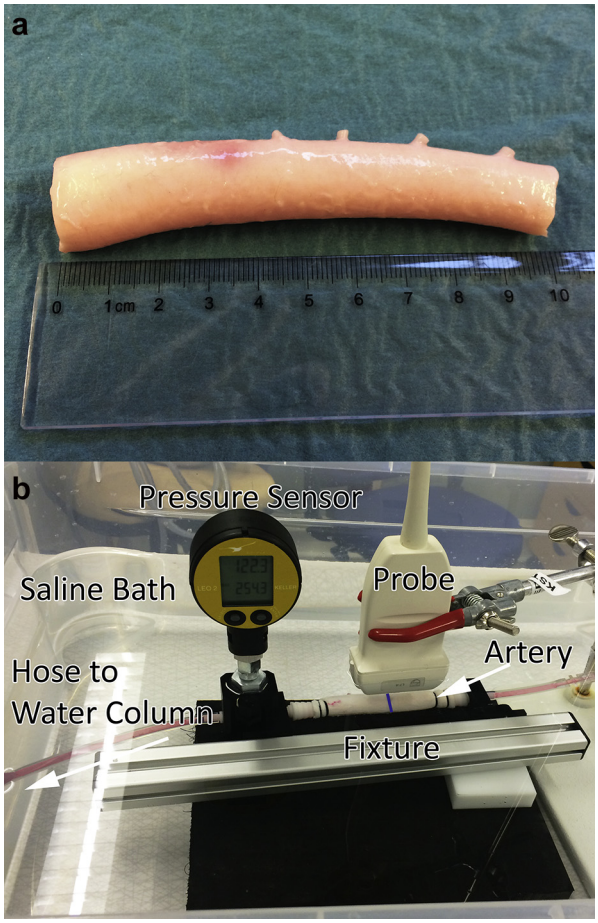

Fig. 1. (a) Porcine thoracic aorta with intercostal arterioles facing upward. (b) Artery with *a blue center line* to visually distinguish the unstiffened arterial wall and simulated plaque. The artery is connected to a fixture with an attached pressure sensor connected to a saline-filled water column while the fixture is placed in a saline bath. The fixed probe generates shear waves and collects in-phase and quadrature data in the arterial wall (left of the *blue center line*) and simulated plaque (right of the *blue center line*).

frequency: 4.09 MHz) with an *F*-number of 1, and the resulting propagating shear wave was measured with high-speed plane wave imaging with a center frequency of 5 MHz (Fig. 2). The ARF push had a lower center frequency than the imaging center frequency to reduce attenuation of the push pulse (Amador Carrascal et al. 2016; Palmeri et al. 2008). Moreover, it is beneficial to image at higher frequencies to achieve higher spatial resolution and, thus, better accuracy in the motion estimation (Dhanaliwala et al. 2012). A 180-V peak-to-peak imaging and push voltage was applied to the transducer. The anterior wall slightly to the left of the highlighted arterial midpoint was excited, and the left propagating shear wave was measured for the unstiffened arterial wall. For the simulated plaque, the anterior wall slightly to the right of the artery's highlighted midpoint was excited, and the right propagating shear wave was measured (Fig. 1b). Data were collected separately in the unstiffened part of the arterial wall and the simulated plaque for all experiments. After each ARF push, 10 ms of high-speed plane wave imaging data (frame rate 10 kHz) were collected to capture the shear wave propagation. Three data acquisitions were collected for all measurements from which the mean and standard deviation were computed.

For the push length analysis, data were collected at 60 and 120 mmHg in the arterial wall and simulated plaque as the push length was varied from 100 to 700 μs in 100-μs increments while the resulting bandwidth and shear modulus were measured. In this article, bandwidth is defined as all frequencies below the frequency at which the first discontinuity occurs in the phase velocity curve.

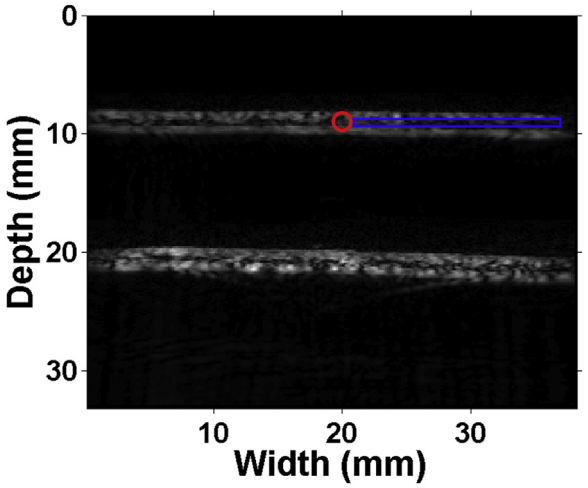

Fig. 2. B-Mode image (Verasonics) of porcine artery 2 at 60 mmHg pressurization submerged in saline. The *red circle* indicates the pushing location, and the *blue region* of interest indicates the area where the shear wave propagation speed was measured. The simulated plaque is located to the right of the push location, and the normal arterial wall is to the left.

The push length that resulted in the widest bandwidth was used in the angle compounding, pressure and sensitivity experiments.

To study the relationship between number of compounded angles and bandwidth, the push length was selected based on the push length analysis, and data were collected at 60 and 120 mmHg while the number of compounded angles was varied from 1 to 3 to 5. For 3 and 5 compounded angles, the imaging angles were $[-1, 0, 1]^\circ$ and $[-2, -1, 0, 1, 2]^\circ$, respectively. The shear wave bandwidth was measured, and the number of angles that resulted in the widest bandwidth was used in the pressure and sensitivity experiments.

Data were collected from 20 to 120 mmHg in 20-mmHg increments for the pressure experiment, and the shear modulus was estimated. The upper limit of the bandwidth was fixed at 1700 Hz such that all shear modulus estimates would be evaluated over the same bandwidth. The upper limit was empirically selected from initial testing based on the minimum bandwidth obtained in the arterial wall and plaque for all pressures. The pressure experiment was repeated on five arteries.

To determine the sensitivity of the SWE technique, an artery was repeatedly soaked in formaldehyde from 0 to 10 min using 2-min intervals, and the arterial wall shear modulus was estimated at 60 mmHg. For each interval, the artery was removed from the fixture, soaked in formaldehyde and then reattached to the fixture in the previously described experimental setup. The bandwidth upper limit was fixed at 1700 Hz for the evaluation of shear moduli. Table 1 summarizes all of the experimental setups.

Image analysis

The IQ data were post-processed in MATLAB 2012b (The MathWorks, Natick, MA, USA) using an in-house post-processing algorithm (Widman et al. 2015b). A summary of the algorithm is provided, but the reader is referred to the reference for a detailed description. The shear wave motion was tracked using a 2-D autocorrelator (Loupas et al. 1995), and the arterial wall tissue displacement was measured along three lateral pixel lines and averaged together to reduce noise. The resulting data were plotted in spatiotemporal displacement plots.

After the shear wave had fully propagated, temporal data along the time axis were cropped out to remove late wall reflections and noise. Next, the *k*-space representation of the signal was obtained by performing a 2-D fast Fourier transform on the spatiotemporal matrix. The *k*-space plot was cropped to the upper right (right propagating wave) or lower right (left propagating wave) quadrant depending on the direction of propagation for the analyzed wave. Noise was removed by an amplitude

mask set to retain 97% of the maximum signal intensity. A phase velocity (c_p) plot was computed as

$$c_p = \lambda f \tag{5}$$

where λ is the wavelength, and f is the frequency of the shear wave. The phase velocity curve for the dominant asymmetric Lamb wave mode was obtained by finding the maximum magnitude for each frequency. The equation for an anti-symmetric Lamb wave propagating in a thin plate (eqn 2) was fit, using a least-squares method, to the upper half-bandwidth of the phase velocity data from which the shear modulus (μ) was estimated. The shear modulus was varied in the plate model $y(\mu)_i$ with a step size of 1 kPa until the error (R^2) between the model and phase velocity was minimized:

$$\min_{\mu} R^2 = \sum \left[y(\mu)_i - c_p(f_i, f_1, f_2, \ldots, f_n) \right]^2 \tag{6}$$

The arterial wall and plaque thickness were used as input parameters in fitting the model to the phase velocity in the post-processing algorithm. The algorithm has been validated in arterial phantoms and has a maximum estimation error of approximately 10% in the same range of pressurization (Maksuti et al. 2016).

For the pressure experiment, the quality of the curve fits was evaluated by calculating the root mean square error (RMSE) between the shear wave phase velocity curve and Lamb wave curve fit as

$$\mathrm{RMSE} = \sqrt{\sum_{n=1}^{N} \frac{\left(c_p(n) - c_L(n)\right)^2}{N}} \tag{7}$$

where $c_p(n)$ is the measured phase velocity, $c_L(n)$ is the curve fit of the Lamb wave propagation speed and N is the number of data samples.

For the angle compounding experiment, the image quality in the anterior arterial wall was evaluated by calculating the mean and standard deviation of the SNR on the radiofrequency data for the three data acquisitions. The SNR was calculated as

$$\mathrm{SNR} = 10 \log_{10} \left\{ \left(\frac{\mathrm{Signal}_{\mathrm{RMS}}}{\mathrm{Noise}_{\mathrm{RMS}}} \right)^2 \right\} \tag{8}$$

where $\mathrm{Noise}_{\mathrm{RMS}}$ is the root mean square (RMS) of the background noise measured in the saline above the artery, and $\mathrm{Signal}_{\mathrm{RMS}}$ is the RMS of the signal from the upper wall.

RESULTS

The average artery length was 9.68 ± 0.32 cm, and wall thickness, plaque thickness and lumen diameter are listed in Table 2. The results from the push length analysis in the arterial wall and plaque can be seen in Figure 3 for 60 mmHg (a) and 120 mmHg (b). Peak bandwidths of 1920 ± 5 and 2030 ± 15 Hz were achieved in the wall and plaque, respectively, at a push length of 100 μs. In the wall, the largest reduction in bandwidth occurred between 400 and 500 μs, whereas the largest reduction of bandwidth in the plaque occurred between 200 and 300 μs. The minimum bandwidths were 925 ± 39 and 993 ± 6 Hz for the wall at 60 mmHg and plaque at 120 mmHg, respectively, measured at a push length of 700 μs. Figure 3(b, d) illustrates that it is more important to have a short push length in the plaque at systolic pressures to obtain a large bandwidth and a reliable shear modulus estimate compared with diastolic pressures (Fig. 3a, c). This is because the shear modulus estimates in the plaque at systolic pressures (Fig. 3d) increase at a greater rate for push lengths from 100 to 400 μs compared with the shear modulus estimates in the plaque at diastolic pressures (Fig. 3c). The greater rate in shear modulus overestimation in the plaque for systolic pressures can be attributed to the faster propagation of the shear wave in the stiffened region at higher pressures, making it more difficult to track. Figure 3(c, d) illustrates that the shear modulus can be significantly overestimated if the shear wave bandwidth is limited.

The results indicate the importance of achieving a large bandwidth when estimating the shear modulus in stiff materials, such as a stiff plaque at systolic pressures, to obtain a consistent estimate. On the basis of the results, a push length of 100 μs was selected for the angle compounding, pressure and sensitivity experiments. The ARF push length results apply to other ARF push center frequencies as well, assuming that the ARF push is not attenuated at higher frequencies and that a sufficient ARF can be produced at the selected center frequency to generate a measurable shear wave that will propagate throughout the wall or plaque. In practice, the tissue does not have time to respond to the ultrasound cycles but does respond to the overall push length of the ARF.

Table 2. Artery wall thickness, plaque thickness and lumen diameter*

Artery	Wall thickness (mm)	Plaque thickness (mm)	Lumen diameter (mm)
1	1.17 ± 0.02†	1.44 ± 0.01	8.50 ± 0.10
2	1.23 ± 0.04	1.46 ± 0.03	8.68 ± 0.20
3	1.49 ± 0.06	2.02 ± 0.03	12.23 ± 0.37
4	1.60 ± 0.00	1.33 ± 0.06	12.23 ± 0.13
5	1.23 ± 0.05	1.35 ± 0.07	12.22 ± 0.23

* Wall thickness and plaque thickness are averaged over the pressurized range 20 to 120 mmHg. Lumen diameter was measured at 60 mmHg.

† Mean ± standard deviation.

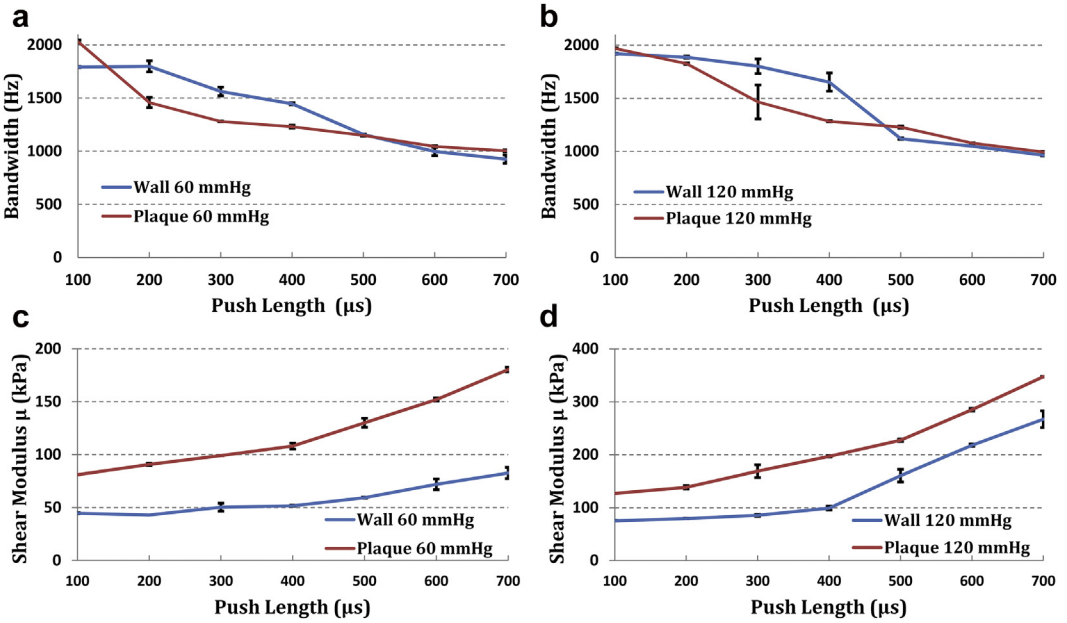

Fig. 3. Shear wave bandwidth with respect to the acoustic radiation force impulse length (push length) for the arterial wall (*blue line*) and plaque (*red line*) at 60 mmHg (a) and 120 mmHg (b) in artery 1. (c, d) Resulting shear modulus estimations with respect to push length for the bandwidths in (a) and (b) at 60 and 120 mmHg, respectively. The *black error bars* indicate the standard deviations for the shear wave bandwidth measurements in (a) and (b) and shear modulus estimates in (c) and (d).

Therefore, the push length results can be applied to other ARF center frequencies.

Figure 4 illustrates the shear wave bandwidth with respect to the number of compounded imaging angles in the arterial wall and plaque at 60 and 120 mmHg. The imaging PRFs were 10,000, 3333 and 2000 Hz for one, three and five imaging angles, respectively. From one to three imaging angles, reductions of approximately

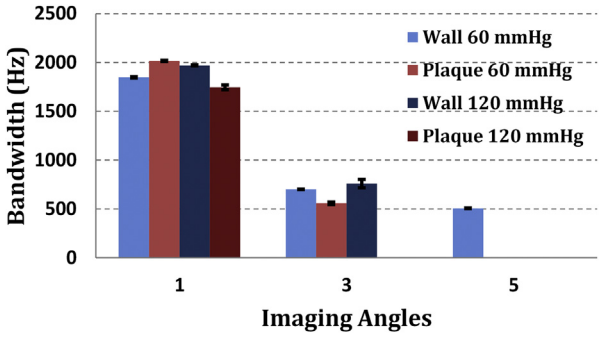

Fig. 4. Shear wave bandwidth with respect to the number of compounded imaging angles for the arterial wall and plaque at 60 and 120 mmHg. The pulse repetition frequency was not sufficient to track the shear wave for the arterial wall at 120 mmHg at five compounded angles and for the plaque at 60 mmHg at five compounded angles and 120 mmHg at three and five compounded angles. The *black error bars* indicate the standard deviations for the shear wave bandwidth measurements.

1200 and 1500 Hz occur in the wall and plaque, respectively, as a result of the reduced PRF. It was not possible to track the shear wave in the arterial wall at 120 mmHg with five imaging angles; that in the plaque at 60 mmHg with five imaging angles; or that in the plaque at 120 mmHg with three or five imaging angles because of the low PRF. On the basis of the results, one imaging angle was selected for the pressure and sensitivity experiments. The means and standard deviations of the SNRs in the vessel wall and plaque with respect to the number of imaging angles at 60 mmHg are listed in Table 3.

The shear modulus estimates with respect to pressure in the arterial wall and plaque for five arteries, denoted as A1–A5, are illustrated in Figure 5(a, b). Compared with the arterial wall, the plaque increases in stiffness at a greater rate with respect to pressure. Sample

Table 3. Signal-to-noise ratios for arterial wall and plaque with respect to number of imaging angles at 60 mmHg

	Signal-to-noise ratio (dB)	
No. of imaging angles	Wall	Plaque
1	44.7 ± 0.5*	46.5 ± 0.3
3	45.7 ± 0.1	47.3 ± 0.3
5	46.3 ± 0.3	48.7 ± 0.2

* Mean ± standard deviation.

phase velocity curves from A2 of the shear wave propagating in the arterial wall and plaque are plotted in Figure 5(c and d, respectively). Note that the overshoot at 500 Hz increases with pressure in the wall, whereas the plaque does not exhibit the same response with increasing pressure.

Figure 6 gives sample spatiotemporal axial displacement plots for the shear wave propagating through the arterial wall (a) and plaque (b) for A2 pressurized at 60 mmHg with peak displacements of approximately 2 μm traveling a distance of 19 mm. The slope of the wave indicates the propagation speed, which indicates a faster wave traveling through the plaque than through the arterial wall. The corresponding curve fits between the Lamb wave model and the upper half-bandwidth of the phase velocity curve can be seen in Figure 6(c, d) for the arterial wall and plaque, respectively. The means and standard deviations of the RMSEs between the Lamb wave curve fit and shear wave phase velocity data for the arterial wall and plaque are listed in Table 4. The RMSE increases with respect to pressure, indicating there is more error in the shear modulus estimates at higher pressures. The shear wave velocity increases with respect to pressure, leading to fewer frames that capture the shear wave propagation motion, resulting in noisier data that increased the RMSE. It has been reported that errors increase in stiffer materials (Wang et al. 2013).

The shear modulus estimates with respect to the time in which the artery soaked in formaldehyde can be seen in Figure 7. The SWE technique can detect a small change in stiffness after 2 min and a larger change after 4 min.

DISCUSSION

Quantifying arterial wall and plaque stiffness is critical for detecting early-onset atherosclerosis and quantitatively assessing plaque vulnerability. Detecting physiologic changes in the arterial wall is crucial to early intervention, and quantitative plaque characterization is necessary to determine the most suitable treatment for patients with carotid plaques, as treatment options can vary depending on plaque composition, location and morphology (Easton and Wilterdink 1994). Ultrasound-based SWE has the potential to become a widely available non-invasive technique for quantitative plaque assessment, complementing the current clinical standard of first-level ultrasound-based visual assessment of the degree of lumen stenosis. Moreover, SWE phase velocity analysis has been reported to provide reliable estimates of plaque stiffness in a phantom setup in contrast to time of flight-based estimations (Widman et al. 2015b).

The push length analysis revealed three important findings. First, Figure 3(c, d) illustrates that it was possible to obtain consistent estimates in the arterial wall with bandwidths as low as approximately 1500 Hz

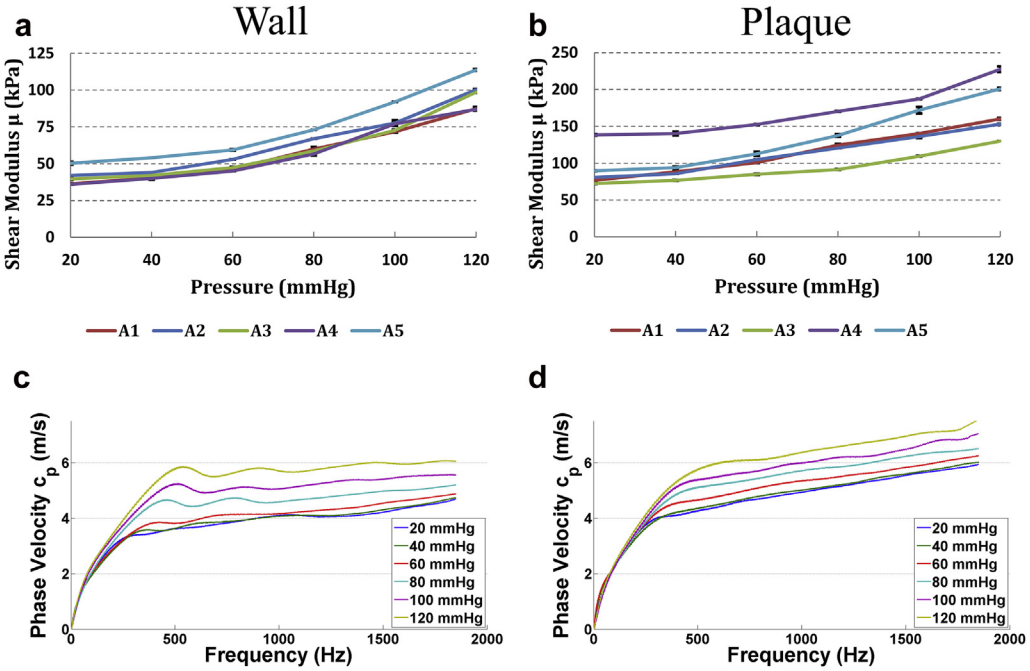

Fig. 5. Shear modulus estimates (kPa) with respect to lumen pressure (mmHg) for the arterial wall (a) and plaque (b) in five arteries labeled A1–A5. The *black error bars* indicate the standard deviations for the shear modulus estimates. Sample phase velocity curves for 20–120 mmHg in the arterial wall (c) and plaque (d) in A2.

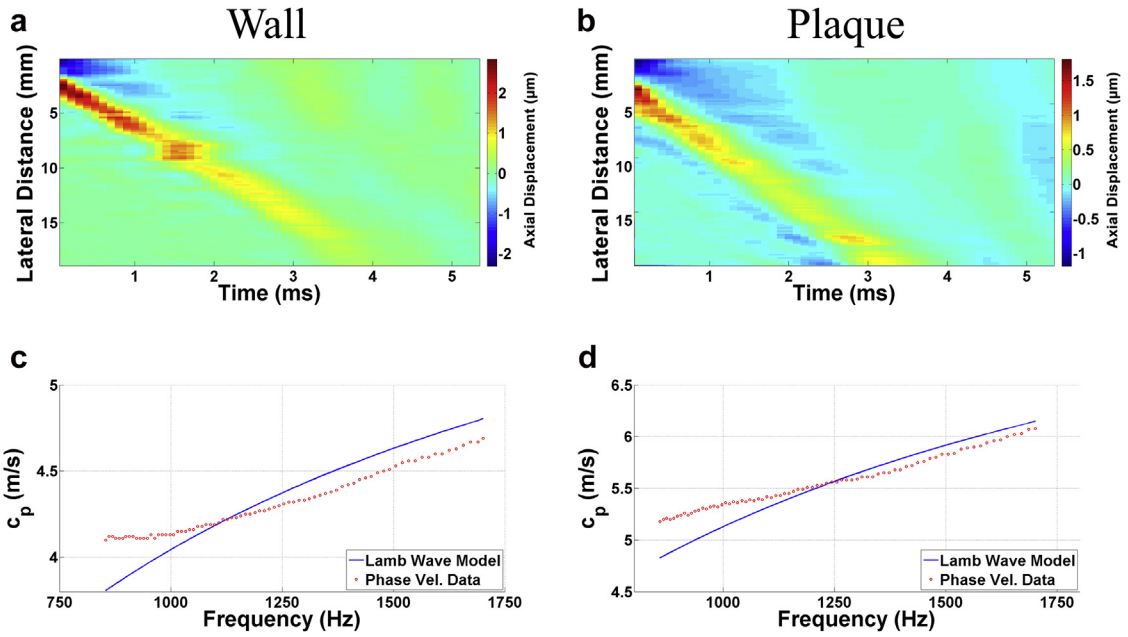

Fig. 6. Sample spatiotemporal axial displacement plots of the shear wave propagating through the arterial wall (a) and plaque (b) with corresponding Lamb wave model curve fits (*blue lines*) to the shear wave phase velocity data (*red dots*) on the upper half-bandwidth of the phase velocity curve (c, d) for artery 2 pressurized at 60 mmHg.

(Fig. 3a, b). The shear modulus estimate increases rapidly when using push lengths longer than 300 μs, which results in bandwidths less than 1500 Hz. Second, Figure 3(a, c) illustrates that it is more difficult to obtain a consistent estimate in the simulated stiff plaque, as the bandwidth drops faster with respect to push length compared with the arterial wall. Similar to the wall, a bandwidth of approximately 1500 Hz is required for a consistent shear modulus estimate in the plaque. Third, Figure 3(b, d) illustrates that a larger bandwidth is required for stiff plaques at high pressures to obtain consistent shear modulus estimates. This corresponds to the increasing RMSE with respect to pressure in Table 4.

The compounded angle experiment indicates that having a high PRF is more important than increasing the image quality at the expense of a reduced PRF when tracking shear waves, especially in stiff tissue such as stiff plaques or wall regions with increased arterial stiffness. This is not an intuitive result, as it is difficult to estimate which factor is more important. Table 3 indicates that the SNR in the wall and plaque marginally increased with the number of compounded angles at the expense of a reduced PRF. The improvement in SNR may be greater *in vivo* because of the scattering tissues surrounding the artery. Figure 4 illustrates that it was not possible to track the shear wave propagation at three imaging angles for the plaque at 120 mmHg. It was only possible to track the shear wave propagating through the wall at 60 mmHg at five imaging angles. The bandwidth was drastically

Table 4. Root mean square error between the lamb wave curve fit and shear wave phase velocity data for the arterial wall and plaque

	Root mean square error (m/s)	
Pressure (mmHg)	Wall	Plaque
20	0.148 ± 0.025*	0.079 ± 0.039
40	0.113 ± 0.049	0.110 ± 0.040
60	0.124 ± 0.056	0.137 ± 0.041
80	0.222 ± 0.128	0.166 ± 0.065
100	0.239 ± 0.072	0.187 ± 0.060
120	0.322 ± 0.022	0.281 ± 0.030

* Mean ± standard deviation.

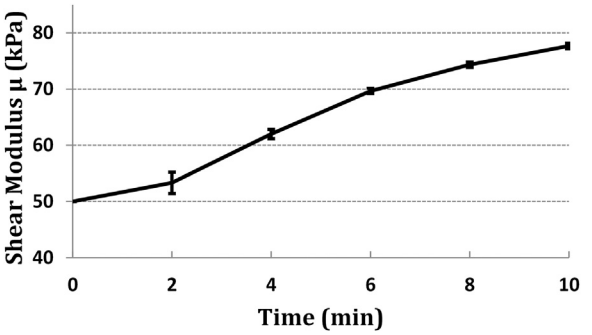

Fig. 7. Shear modulus estimates (kPa) with respect to the time (min) the artery soaked in formaldehyde measured at 60 mmHg. The *black error bars* indicate the standard deviations for the shear modulus estimates.

reduced approximately 1500 Hz, and it was not possible to obtain reliable shear modulus estimates, as seen in the results from the push length analysis. It is important to note that the shear wave bandwidth is not decreasing with respect to the number of compounded imaging angles. Instead, the algorithm's ability to measure the bandwidth of the propagating shear wave is decreased because of the reduction in imaging frame rate, which increases the noise in the shear wave spatiotemporal plots. It may be possible to overcome the decrease in frame rate caused by compounding by interleaving the data, which will be explored in future work.

The pressure experiment indicated one important finding. For typical *in vivo* pressures ranging from 60 to 120 mmHg, the shear modulus response of the artery with respect to pressure was approximately linear. Expressing the relationship as

$$\mu_p = kP + b \tag{9}$$

where μ_p is the phase velocity estimated shear modulus of the artery (kPa), k is the slope of the regression, P is the arterial lumen pressure (mmHg) and b is the zero pressure intercept (mmHg). Applying the linear regression to the wall and plaque data for the five arteries yields

$$\mu_{p\ wall} = 0.784P + 1.66 \quad 60 \leq P \leq 120 \tag{10}$$

$$\mu_{p\ plaque} = 1.081P + 45.32 \quad 60 \leq P \leq 120 \tag{11}$$

with sums of squared errors of 2.94 and 11.85 kPa for the wall and plaque, respectively.

The models can be used for simulations of cardiovascular dynamics and provide estimates of arterial wall and plaque shear moduli. The linear response in arterial stiffness with respect to pressure is in agreement with Bergel (1961), who observed an approximately linear relationship between Young's modulus and static pressure in canine thoracic aortas for pressures up to 120 mmHg. It is unknown if the linear relationship holds for *in vivo* conditions, as the experiment was performed *ex vivo* with static pressures with no surrounding tissues. Based on the results of Bergel (1961) and Couade et al. (2010), it is likely that the dynamic *in vivo* environment, with rapid changes in pressure, would induce a non-linear elastic response in the arterial wall.

The increase in shear modulus with respect to pressure differs from previous studies. Bernal et al. (2011) performed a similar experiment measuring the shear modulus with respect to static pressure in porcine carotid arteries from 10 to 100 mmHg and obtained relatively constant shear moduli that decreased slightly as the pressure increased. However, Couade et al. (2010) measured the shear modulus in the carotid artery wall *in vivo* of a healthy human in whom stiffness varied between 130 ± 15 kPa in systole and 80 ± 10 kPa in diastole (the blood pressure was not provided), which is in agreement with our results of 97 ± 10 kPa at 120 mmHg and 50 ± 5 kPa at 60 mmHg (Fig. 5a). The results from Couade et al. (2010) fall between our results for the wall and simulated plaque, which can be expected because we are comparing porcine aortas and human carotid arteries. Furthermore, Couade et al. (2010) measured a difference of approximately 50 kPa in wall stiffness for the healthy arterial wall throughout the cardiac cycle, which matches our difference of 56 kPa in wall stiffness between systolic and diastolic pressures. Schmitt et al. (2010) measured 5–17 kPa from 240 to 480 Hz in a porcine abdominal aorta using dynamic micro-elastography with harmonic shear wave propagation. A direct comparison is difficult, as Schmitt et al. (2010) measured in the radial direction of the artery as opposed to the longitudinal direction as in our study, and arteries are known to be anisotropic (Dobrin 1986).

It has been reported that arteries are viscoelastic (Schmitt et al. 2010), and analytical solutions for viscoelastic vessel models are the focus of our future work. The focus of our study was to optimize measurements for elastic vascular characterizations.

Fitting a Lamb wave dispersion equation for a homogeneous elastic plate submerged in incompressible water-like fluid to the shear wave phase velocity data can be questioned, but several studied have used this model (Bernal et al. 2011; Couade et al. 2010), and the results have been validated against mechanical testing (Maksuti et al. 2016; Widman et al. 2015b). Initial results indicate that the model works *in vivo* as well, where the arteries are surrounded by tissue (Couade et al. 2010). Better shear wave propagation models are needed in the future, but the Lamb wave model is currently the best available model for estimating the shear modulus in arteries or plaque.

The thickness of the wall and stiff plaque model was measured at three locations throughout the shear wave propagation region and averaged (Table 2) to account for variation in wall and plaque thickness, as it is an important parameter in the Lamb wave propagating through an infinite plate model. The sensitivity of the model with respect to plaque or wall thickness has not been studied systematically, but will be included in future work. Currently, the Lamb wave model is the most reliable model available. *In vivo* plaques with variation in thickness caused by surface irregularities and morphologic variation can be accounted for by acquiring and averaging multiple measurements within the shear wave propagation region. Alternatively, multiple shear modulus estimates could be performed in regions of varying thickness.

The sensitivity experiment revealed one important result. Figure 7 illustrates the capability of SWE to detect

small stiffness changes in the artery, potentially allowing for the detection of small changes in arterial wall stiffness to be used as the clinical standard for early detection of atherosclerosis. The new biomarker could potentially allow for earlier detection compared with intima–media thickness, assuming that a physiologic change in stiffness occurs before a visually detectable thickening of the arterial wall. Moreover, the ability to detect small changes in plaque stiffness suggests that SWE may be suitable for plaque characterization. Additionally, Figure 7 illustrates that the artery increases in stiffness non-linearly when soaked in formaldehyde. The stiffness increases marginally the first 2 min, increases at the fastest rate from 2 to 6 min, then slows down from 6 to 10 min, creating a "S-shape" in the shear modulus-versus-time line plot. The slow start to the stiffening could be due to the diffusion of the formalin within the microvessels in the adventitia layer to the smooth muscle in the tunica media. The stiffening saturates over time, reducing the effect of the formaldehyde. The stiffness values are in agreement with the shear modulus curves in Figures 5(a, b). Data for the sensitivity experiment were collected at 60 and 120 kPa, but the data at 120 kPa suffered from poor quality because of arterial buckling from the high pressure and were omitted.

A recent pilot study successfully characterized carotid plaque in four humans using ARFI imaging (Czernuszewicz et al. 2015), a similar elastography technique that measures the relative tissue displacement to nearby surrounding tissue, rather than the speed of the resulting propagating shear wave. However, it is still unknown if SWE or ARFI imaging is more suitable for plaque characterization, as the results must be validated in a larger study to statistically correlate the ARFI-derived plaque characteristics to the patients' symptoms. Tolerability must be taken into consideration when exciting plaques with ARF to avoid plaque rupture. A simulation has indicated that the blood pressure exerts three orders of magnitude more stress on the plaque compared with ARF (Doherty et al. 2013a). Both SWE (Garrard et al. 2015) and ARFI (Czernuszewicz et al. 2015) have been attempted on *in vivo* carotid plaques with no reported complications.

Some experimental limitations of the study deserve to be pointed out. It was not possible to obtain arteries with real plaques. Only stiffened arteries aimed to simulate increased arterial stiffness or homogeneous stiff plaques located in the arterial wall were included in the study because of the limitations of the plaque fabrication technique. However, unlike real plaques, the morphology did not change. It is important to note that the simulated stiff plaque model used in this study does not reflect a typical vulnerable plaque with a necrotic core and a thin fibrous cap. SWE will be more difficult on plaques with complicated geometry that protrudes into the arterial lumen, often described as vulnerable plaques, but our algorithm has successfully measured soft vulnerable plaque phantoms of this type (Widman et al. 2015b). Phase velocity analysis may be most suitable for homogeneous plaques and must be further developed for plaques of heterogeneous composition.

The experiment was also performed with a static pressure. However, the technique has previously successfully estimated the stiffness in a geometrically realistic soft plaque phantom with dynamic pressures (Widman et al. 2015b). The porcine aorta intima–media–adventitia thickness (Table 2) was slightly thicker than human carotid intima–media thickness (approximately 0.8 mm) reported in literature (Onut et al. 2012), which was expected because the adventitia layer was still intact. The aorta was selected as the artery of choice because of its availability, as porcine carotid arteries were not available. Short-axis imaging was not included as only the shear wave propagating along the long axis was considered in this study. This is a potential topic for future studies, as arteries are known to be anisotropic (Dobrin 1986). The shear wave propagation was tracked along a straight pixel line, and another potential future study would be to track the wave along a curved surface to allow for easier *in vivo* implementation when estimating arterial stiffness. A clinical implementation will be more difficult than the experimental setup for two reasons. First, in this experiment, the artery was placed in a saline bath, where it is likely to achieve more bandwidth than if it was surrounded by tissue. Second, it is unknown if a 100-μs push will generate a strong enough wave at a 1- to 2-cm depth with overlying tissue. Moreover, the SNR will deteriorate because of surrounding tissues. These are topics for future *in vivo* studies.

CONCLUSIONS

The shear modulus was successfully estimated in five arteries with simulated increased arterial stiffness or a stiff plaque model using SWE, where a linear response in stiffness with respect to realistic *in vivo* diastolic and systolic pressures was found. A minimum bandwidth of approximately 1500 Hz is necessary for consistent shear modulus estimates using phase velocity analysis, and a 100-μs push length results in the largest bandwidth. Moreover, a high PRF with poorer image quality is more important than a lower PRF with better image quality when estimating arterial wall and plaque stiffness using SWE. The results illustrate the ability of SWE to characterize the mechanical properties of arterial walls and plaques and the potential for SWE to become a non-invasive technique for quantitative plaque assessment, as well as detection of early-onset atherosclerosis.

Acknowledgments—This study was supported by Swedish Research Council Grant 2012-2795. We thank Pellina Janson at Karolinska Experimental Research and Imaging Centre (KERIC), Karolinska University Hospital, Sweden, for providing porcine aortas for the experiments.

REFERENCES

Allen JD, Ham KL, Dumont DM, Sileshi B, Trahey GE, Dahl JJ. The development and potential of acoustic radiation force impulse (ARFI) imaging for carotid artery plaque characterization. Vasc Med 2011;16:302–311.

Amador Carrascal C, Aristizabal Taborda S, Greenleaf J, Urban M. Phase aberration and attenuation effects on acoustic radiation force-based shear wave generation. IEEE Trans Ultrason Ferroelectr Freq Control 2016;63:222–232.

Barnett HJ, Taylor DW, Eliasziw M, Fox AJ, Ferguson GG, Haynes RB, Rankin RN, Clagett GP, Hachinski VC, Sackett DL, Thorpe KE, Meldrum HE, Spence JD, for the North American Symptomatic Carotid Endarterectomy Trial Collaborators. Benefit of carotid endarterectomy in patients with symptomatic moderate or severe stenosis. N Engl J Med 1998;339:1415–1425.

Bergel DH. The static elastic properties of the arterial wall. J Physiol 1961;156:445–457.

Bernal M, Nenadic I, Urban MW, Greenleaf JF. Material property estimation for tubes and arteries using ultrasound radiation force and analysis of propagating modes. J Acoust Soc Am 2011;129:1344–1354.

Caro CG, Harrison GK. Observations on pulse wave velocity and pulsatile blood pressure in the human pulmonary circulation. Clin Sci 1962;23:317–329.

Carr S, Farb A, Pearce WH, Virmani R, Yao JS. Atherosclerotic plaque rupture in symptomatic carotid artery stenosis. J Vasc Surg 1996;23:755–765. discussion 765–766.

Couade M, Pernot M, Prada C, Messas E, Emmerich J, Bruneval P, Criton A, Fink M, Tanter M. Quantitative assessment of arterial wall biomechanical properties using shear wave imaging. Ultrasound Med Biol 2010;36:1662–1676.

Czernuszewicz TJ, Homeister JW, Caughey MC, Farber MA, Fulton JJ, Ford PF, Marston WA, Vallabhaneni R, Nichols TC, Gallippi CM. Non-invasive in vivo characterization of human carotid plaques with acoustic radiation force impulse ultrasound: Comparison with histology after endarterectomy. Ultrasound Med Biol 2015;41:685–697.

Davis NE. Atherosclerosis—An inflammatory process. J Insur Med 2005;37:72–75.

Dhanaliwala AH, Hossack JA, Mauldin FW. Assessing and improving acoustic radiation force image quality using a 1.5-D transducer design. IEEE Trans Ultrason Ferroelectr Freq Control 2012;59:1602–1608.

Dillman JR, Chen S, Davenport MS, Zhao H, Urban MW, Song P, Watcharotone K, Carson PL. Superficial ultrasound shear wave speed measurements in soft and hard elasticity phantoms: Repeatability and reproducibility using two ultrasound systems. Pediatr Radiol 2015;45:376–385.

Dobrin PB. Biaxial anisotropy of dog carotid artery: Estimation of circumferential elastic modulus. J Biomech 1986;19:351–358.

Doherty JR, Dumont DM, Trahey GE, Palmeri ML. Acoustic radiation force impulse imaging of vulnerable plaques: A finite element method parametric analysis. J Biomech 2013a;46:83–90.

Doherty JR, Trahey GE, Nightingale KR, Palmeri ML. Acoustic radiation force elasticity imaging in diagnostic ultrasound. IEEE Trans Ultrason Ferroelectr Freq Control 2013b;60:685–701.

Dunmore BJ, McCarthy MJ, Naylor AR, Brindle NP. Carotid plaque instability and ischemic symptoms are linked to immaturity of microvessels within plaques. J Vasc Surg 2007;45:155–159.

Easton JD, Wilterdink JL. Carotid endarterectomy: Trials and tribulations. Ann Neurol 1994;35:5–17.

Garrard JW, Ummur P, Nduwayo S, Kanber B, Hartshorne TC, West KP, Moore D, Robinson TG, Ramnarine KV. Shear wave elastography may be superior to greyscale median for the identification of carotid plaque vulnerability: A comparison with histology. Ultraschall Med 2015;36:386–390.

Gennisson JL, Deffieux T, Mace E, Montaldo G, Fink M, Tanter M. Viscoelastic and anisotropic mechanical properties of in vivo muscle tissue assessed by supersonic shear imaging. Ultrasound Med Biol 2010;36:789–801.

Gennisson JL, Grenier N, Combe C, Tanter M. Supersonic shear wave elastography of in vivo pig kidney: influence of blood pressure, urinary pressure and tissue anisotropy. Ultrasound Med Biol 2012;38:1559–1567.

Hamilton PK, Lockhart CJ, Quinn CE, McVeigh GE. Arterial stiffness: Clinical relevance, measurement and treatment. Clin Sci (Lond) 2007;113:157–170.

Kan P, Mokin M, Dumont TM, Snyder KV, Siddiqui AH, Levy EI, Hopkins LN. Cervical carotid artery stenosis: Latest update on diagnosis and management. Curr Probl Cardiol 2012;37:127–169.

Kanber B, Hartshorne TC, Horsfield MA, Naylor AR, Robinson TG, Ramnarine KV. Dynamic variations in the ultrasound greyscale median of carotid artery plaques. Cardiovasc Ultrasound 2013;11:21.

Loree HM, Kamm RD, Stringfellow RG, Lee RT. Effects of fibrous cap thickness on peak circumferential stress in model atherosclerotic vessels. Circ Res 1992;71:850–858.

Loupas T, Powers JT, Gill RW. An axial velocity estimator for ultrasound blood-flow imaging, based on a full evaluation of the Doppler equation by means of a 2-dimensional autocorrelation approach. IEEE Trans Ultrason Ferroelectr Freq Control 1995;42:672–688.

Luo J, Li RX, Konofagou EE. Pulse wave imaging of the human carotid artery: an in vivo feasibility study. IEEE Trans Ultrason Ferroelectr Freq Control 2012;59:174–181.

Mahmoud AM, Dutta D, Lavery L, Stephens DN, Villanueva FS, Kim K. Noninvasive detection of lipids in atherosclerotic plaque using ultrasound thermal strain imaging: In vivo animal study. J Am Coll Cardiol 2013;62:1804–1809.

Maksuti E, Widman E, Larsson D, Urban MW, Larsson M, Bjallmark A. Arterial stiffness estimation by shear wave elastography: Validation in phantoms with mechanical testing. Ultrasound Med Biol 2016;42:308–321.

Maurice RL, Soulez G, Giroux MF, Cloutier G. Noninvasive vascular elastography for carotid artery characterization on subjects without previous history of atherosclerosis. Med Phys 2008;35:3436–3443.

Mehrmohammadi M, Song P, Meixner DD, Fazzio RT, Chen S, Greenleaf JF, Fatemi M, Alizad A. Comb-push ultrasound shear elastography (CUSE) for evaluation of thyroid nodules: Preliminary in vivo results. IEEE Trans Med Imaging 2015;34:97–106.

Montaldo G, Tanter M, Bercoff J, Benech N, Fink M. Coherent plane-wave compounding for very high frame rate ultrasonography and transient elastography. IEEE Trans Ultrason Ferroelectr Freq Control 2009;56:489–506.

Muller HF, Viaccoz A, Kuzmanovic I, Bonvin C, Burkhardt K, Bochaton-Piallat ML, Sztajzel R. Contrast-enhanced ultrasound imaging of carotid plaque neo-vascularization: Accuracy of visual analysis. Ultrasound Med Biol 2014;40:18–24.

Muller M, Gennisson JL, Deffieux T, Tanter M, Fink M. Quantitative viscoelasticity mapping of human liver using supersonic shear imaging: Preliminary in vivo feasibility study. Ultrasound Med Biol 2009;35:219–229.

Naghavi M, Libby P, Falk E, Casscells SW, Litovsky S, Rumberger J, Badimon JJ, Stefanadis C, Moreno P, Pasterkamp G, Fayad Z, Stone PH, Waxman S, Raggi P, Madjid M, Zarrabi A, Burke A, Yuan C, Fitzgerald PJ, Siscovick DS, de Korte CL, Aikawa M, Airaksinen KE, Assmann G, Becker CR, Chesebro JH, Farb A, Galis ZS, Jackson C, Jang IK, Koenig W, Lodder RA, March K, Demirovic J, Navab M, Priori SG, Rekhter MD, Bahr R, Grundy SM, Mehran R, Colombo A, Boerwinkle E, Ballantyne C, Insull W Jr, Schwartz RS, Vogel R, Serruys PW, Hansson GK, Faxon DP, Kaul S, Drexler H, Greenland P, Muller JE, Virmani R, Ridker PM, Zipes DP, Shah PK, Willerson JT. From vulnerable plaque to vulnerable patient: A call for new definitions and risk assessment strategies, Part II. Circulation 2003a;108:1772–1778.

Naghavi M, Libby P, Falk E, Casscells SW, Litovsky S, Rumberger J, Badimon JJ, Stefanadis C, Moreno P, Pasterkamp G, Fayad Z, Stone PH, Waxman S, Raggi P, Madjid M, Zarrabi A, Burke A,

Yuan C, Fitzgerald PJ, Siscovick DS, de Korte CL, Aikawa M, Juhani Airaksinen KE, Assmann G, Becker CR, Chesebro JH, Farb A, Galis ZS, Jackson C, Jang IK, Koenig W, Lodder RA, March K, Demirovic J, Navab M, Priori SG, Rekhter MD, Bahr R, Grundy SM, Mehran R, Colombo A, Boerwinkle E, Ballantyne C, Insull W Jr, Schwartz RS, Vogel R, Serruys PW, Hansson GK, Faxon DP, Kaul S, Drexler H, Greenland P, Muller JE, Virmani R, Ridker PM, Zipes DP, Shah PK, Willerson JT. From vulnerable plaque to vulnerable patient: A call for new definitions and risk assessment strategies, Part I. Circulation 2003b;108:1664–1672.

Onut R, Balanescu AP, Constantinescu D, Calmac L, Marinescu M, Dorobantu PM. Imaging atherosclerosis by carotid intima–media thickness in vivo: How to, where and in whom? Maedica 2012;7: 153–162.

Palmeri ML, Wang MH, Dahl JJ, Frinkley KD, Nightingale KR. Quantifying hepatic shear modulus in vivo using acoustic radiation force. Ultrasound Med Biol 2008;34:546–558.

Quinn U, Tomlinson LA, Cockcroft JR. Arterial stiffness. J R Soc Med Cardiovasc Dis 2012;1:18.

Ramnarine KV, Garrard JW, Dexter K, Nduwayo S, Panerai RB, Robinson TG. Shear wave elastography assessment of carotid plaque stiffness: In vitro reproducibility study. Ultrasound Med Biol 2014;40:200–209.

Saba L, Anzidei M, Marincola BC, Piga M, Raz E, Bassareo PP, Napoli A, Mannelli L, Catalano C, Wintermark M. Imaging of the carotid artery vulnerable plaque. Cardiovasc Intervent Radiol 2014;37:572–585.

Saba L, Anzidei M, Sanfilippo R, Montisci R, Lucatelli P, Catalano C, Passariello R, Mallarini G. Imaging of the carotid artery. Atherosclerosis 2012;220:294–309.

Salem MK, Sayers RD, Bown MJ, West K, Moore D, Robinson TG, Naylor AR. Features of unstable carotid plaque during and after the hyperacute period following TIA/stroke. Eur J Vasc Endovasc Surg 2013;45:114–120.

Schmidt RF, Thews G, (eds). Human physiology. 2nd ed. New York: Springer-Verlag 1989.

Schmitt C, Hadj Henni A, Cloutier G. Ultrasound dynamic microelastography applied to the viscoelastic characterization of soft tissues and arterial walls. Ultrasound Med Biol 2010;36: 1492–1503.

Schwarz F, Bayer-Karpinska A, Poppert H, Buchholz M, Cyran C, Grimm J, Helck A, Nikolaou K, Opherk C, Dichgans M, Saam T. Serial carotid MRI identifies rupture of a vulnerable plaque resulting in amaurosis fugax. Neurology 2013;80:1171–1172.

Song P, Zhao H, Urban MW, Manduca A, Pislaru SV, Kinnick RR, Pislaru C, Greenleaf JF, Chen S. Improved shear wave motion detection using pulse-inversion harmonic imaging with a phased array transducer. IEEE Trans Med Imaging 2013;32:2299–2310.

Tang D, Yang C, Zheng J, Woodard PK, Sicard GA, Saffitz JE, Yuan C. 3-D MRI-based multicomponent FSI models for atherosclerotic plaques. Ann Biomed Eng 2004;32:947–960.

Tanter M, Bercoff J, Athanasiou A, Deffieux T, Gennisson JL, Montaldo G, Muller M, Tardivon A, Fink M. Quantitative assessment of breast lesion viscoelasticity: Initial clinical results using supersonic shear imaging. Ultrasound Med Biol 2008;34:373–386.

Vejdani-Jahromi M, Nagle M, Trahey GE, Wolf PD. Ultrasound shear wave elasticity imaging quantifies coronary perfusion pressure effect on cardiac compliance. IEEE Trans Med Imaging 2015;34: 465–473.

Vlachopoulos C, Aznaouridis K, Stefanadis C. Prediction of cardiovascular events and all-cause mortality with arterial stiffness: A systematic review and meta-analysis. J Am Coll Cardiol 2010;55: 1318–1327.

Wang M, Byram B, Palmeri M, Rouze N, Nightingale K. On the precision of time-of-flight shear wave speed estimation in homogeneous soft solids: Initial results using a matrix array transducer. IEEE Trans Ultrason Ferroelectr Freq Control 2013;60:758–770.

Weizsacker HW, Pinto JG. Isotropy and anisotropy of the arterial wall. J Biomech 1988;21:477–487.

Widman E, Caidahl K, Heyde B, D'Hooge J, Larsson M. Ultrasound speckle tracking strain estimation of in vivo carotid artery plaque with in vitro sonomicrometry validation. Ultrasound Med Biol 2015a;41:77–88.

Widman E, Maksuti E, Larsson D, Urban MW, Bjallmark A, Larsson M. Shear wave elastography plaque characterization with mechanical testing validation: A phantom study. Phys Med Biol 2015b;60: 3151–3174.

World Health Organization. Global atlas on cardiovascular disease prevention and control. Geneva: Author; 2011.

Zhang PF, Su HJ, Zhang M, Li JF, Liu CX, Ding SF, Miao Y, Chen L, Li XN, Yi X, Zhang Y. Atherosclerotic plaque components characterization and macrophage infiltration identification by intravascular ultrasound elastography based on B-mode analysis: Validation in vivo. Int J Cardiovasc Imaging 2011;27:39–49.